Pressure in a Mortar and Estimation of Muzzle Velocity of Expelled Stars

Dayu Ding, Morimasa Higaki, Yuzo Ooki, and Tadao Yoshida*

Ashikaga Institute of Technology
268-1 Omae-cho, Ashikaga-shi, Tochigi 326-8558, Japan
* To whom all correspondence should be addressed
Tel: +81-284-62-0605, fax: +81-284-62-0976, email: yoshida@ashitech.ac.jp

Abstract: *Firing firework star experiments have been carried out using 20 mm and 25 mm inner diameter steel mortars equipped with two or four pressure transducers, and the pressure profiles were recorded. The relative pressure profiles of the four positions in the mortar changed with the gap ratio between sectional areas of the star and the mortar wall, and with the mass of the lifting charge. The maximum pressure attained decreased and the scatter of observed data increased with an increase of the gap ratio. It was shown by experiment using four pressure transducers that, when the gap ratio is large, the pressures to the rear and front of a star should be corrected for the pressure distribution in the mortar.*

In the first half of the experiment, using two pressure transducers the muzzle velocity of a star was estimated from the pressure profile of the bottom transducer. When the gap between star and mortar wall and the mass of lifting charge were small, the calculated and observed muzzle velocities agreed well. However, in the case of a large gap, the calculated value was larger than the observed one.

In the latter half of the experiment, four pressure transducers were used and it was found that in the case of a large gap the pressure profile from the bottom transducer did not give the real pressures to the rear and front of the star in the mortar. A correction for the difference was tried and the agreement between the observed and calculated values was improved.

Keywords: *fireworks, interior ballistics, pressure profile, muzzle velocity*

Introduction

Firework stars are important elements of aerial fireworks. The burning stars fly into the sky and appeal visually to the spectators. The stars are used in two modes. In one mode, stars are packed in a shell with a bursting charge, and ejected into the sky by the deflagration of the bursting charge followed by bursting of the shell. Aerial shell fireworks are examples. In the other mode, stars are fired directly from mortars on the ground. Roman candles and mines are examples.

In the present work, firing star experiments were carried out using mortars equipped with pressure transducers and a high-speed video camera. The inner pressure profiles and the initial velocities of the expelled stars were recorded, and results were analyzed.

A preliminary study was done by the present authors for the inner pressure profiles in the firing stars.[1] K. L. and B. J. Kosanke[2] and Y. Ooki *et al*.[3] have measured inner pressure profiles in the mortar on aerial shell firing, and estimated the muzzle velocity of the shells from the pressure profile.

Experimental

Materials

Stars for no. 2 to no. 10 shells (no. 2.5 shell corresponds to a 3 inch (75 mm) shell) were supplied by the Sunaga Fireworks Co. Ltd., Ashikaga, and the lifting charge and the electric match were made by the Nippon Kayaku Company. The lifting charge is always the same product in Japan and is a grain black powder with the following standards:

Composition (%): potassium nitrate 74–80, sulfur 8–12, charcoal 10–16.
Size (mm) 0.4–1.2
Density (g cm^{-2}) 1.75–1.85

The particle distribution of the lifting charge was determined by us as follows:

<0.15 mm 0%
0.15–0.3 mm 0.03%
0.3–0.6 mm 23.89%
0.6–1.2 mm 76.07%
1.2–2.5 mm 0.01%
>2.5 mm 0%

Apparatus

The two mortars used for firing stars were made of steel, with inner diameters of 20 mm and 25 mm, and depths of 361 mm and 455 mm, respectively. The two mortars were each equipped with two pressure transducers, at the bottom and middle (2/3 from bottom) of the mortar. In the latter experiment, two pressure transducers were added to the 20 mm inner diameter mortar. The dimensions of the mortars with pressure transducers are shown in Figure 1.

The pressure in the mortar during firing was measured using two or four pressure transducers (Kistler 6041A), charge amplifiers (Kistler 5011) and a digital oscilloscope (Sony Tektronix TDS3012 or Yokokawa DL1640 with four channels). The set-up of the pressure measuring system is shown in Figure 2.

The muzzle velocity of the star was measured using a high-speed video camera (Phantom VR-V4.2) with a frame speed of 1000 frames per second.

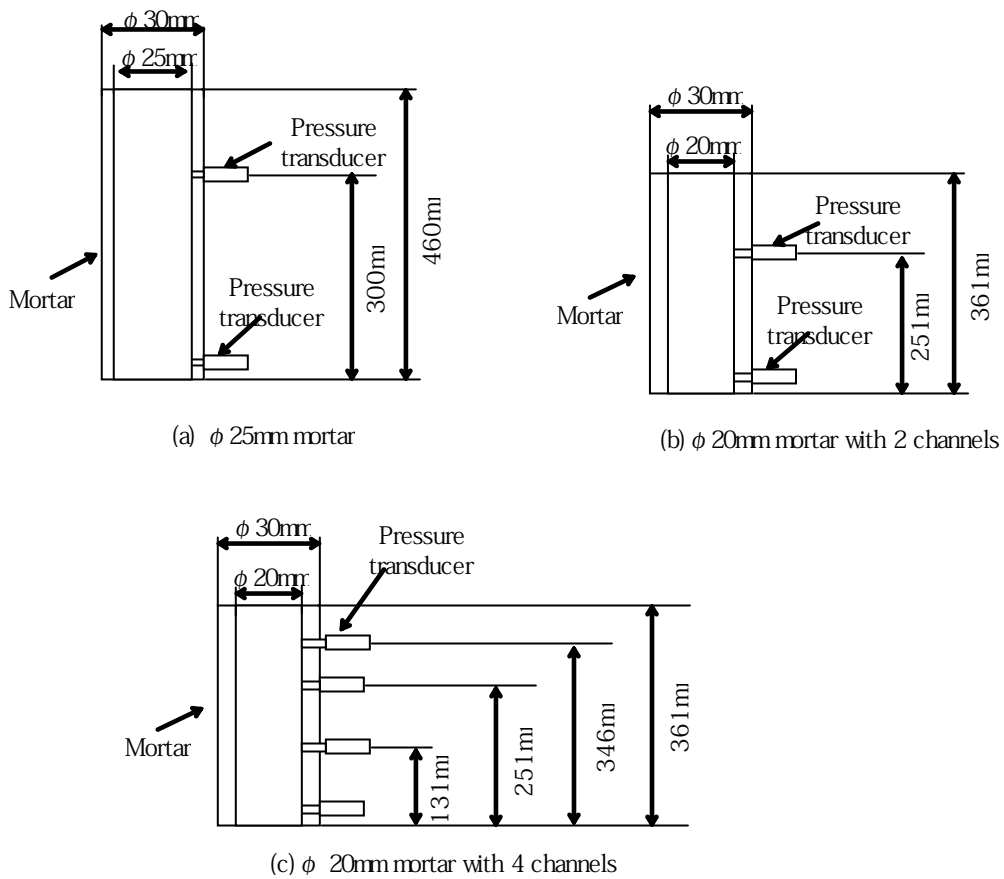

Figure 1. *Mortars and positions of pressure transducers.*

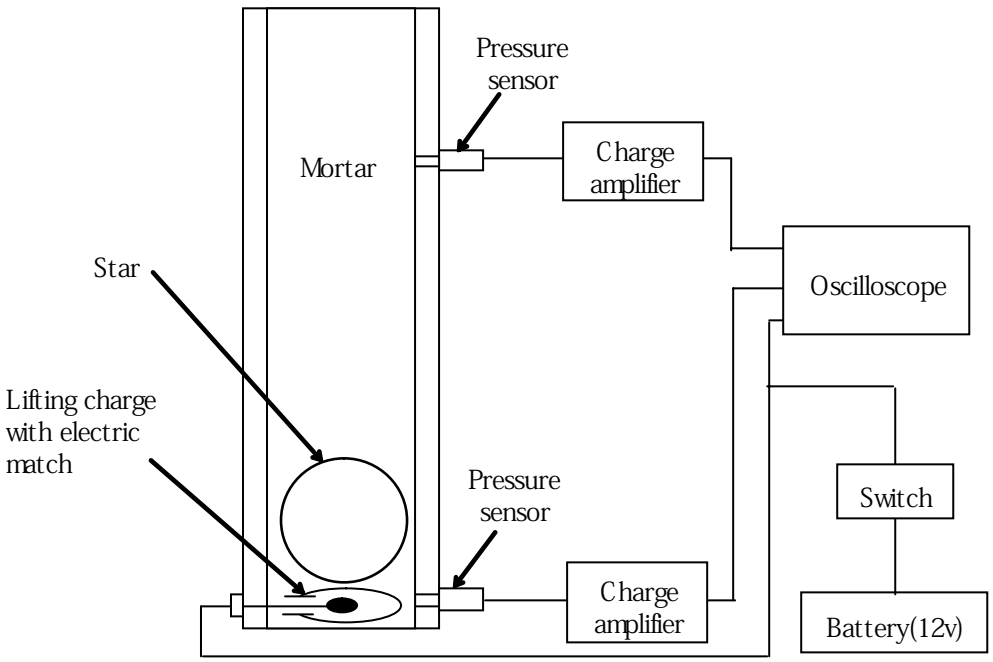

Figure 2. *Setup of the pressure measuring system.*

Procedure

The mortar is set on the ground vertically. The electric match is put in the bottom of the mortar and the lifting charge is poured into the mortar through the muzzle. Then a star is placed on the lifting charge. The electric match is ignited by turning on an electric current. The lifting charge burns, pressure develops and the star moves upwards. The pressure profiles are recorded on an oscilloscope and the initial trajectory of the star in the air is recorded on a high-speed camera. Each frame of the video is reproduced on a video screen and initial velocity of the star is determined.

Results and Discussion

Pressure profile

Examples of the pressure profiles by two pressure transducers in the mortar during shot of the star are shown in Figure 3(a)–(c). Figure 3(a) shows an experimental result with a small lifting charge (LC 0.7 g) and small gap ratio (GR 0.20). Here, the gap ratio is defined as the ratio of the area of the gap between the mortar and the star divided by the area of the mortar.

In the pressure profile at the middle of the mortar, no pressure increase was observed during the first stage of the event. Then, the pressure decreased a little and then increased sharply. The small decrease in pressure may be attributable to the high-speed flow of the combustion gas through the gap between the mortar and the star when the star passed the pressure transducer. The pressures at the bottom and middle transducers decreased sharply after the star left the muzzle. The start time of this sharp decrease at the middle transducer was similar to that at the bottom transducer. This suggests that there is no pressure distribution in the mortar in this case.

Figure 3(b) shows an experiment with a similar GR (0.19) and different LC (2.0 g) compared to Figure 3(a). The pressure at the middle transducer increased a little at first, then decreased a little as in Figure 3(a), and increased sharply. The pressure at the middle transducer after the star passed the transducer was lower than that at the bottom transducer at the same time. This indicates that the pressure behind the star becomes lower higher up, that is, there is a pressure distribution in the space behind the star. The first increase in pressure at the middle transducer shows the pressure increase in front of the star by the combustion gas leaking through the gap between the star and the mortar wall.

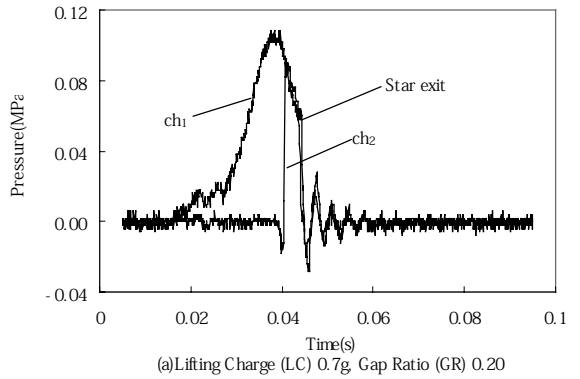

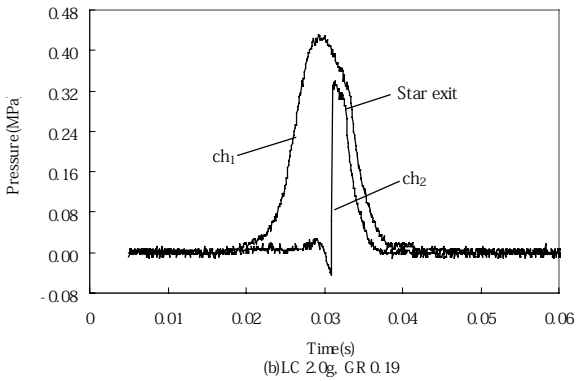

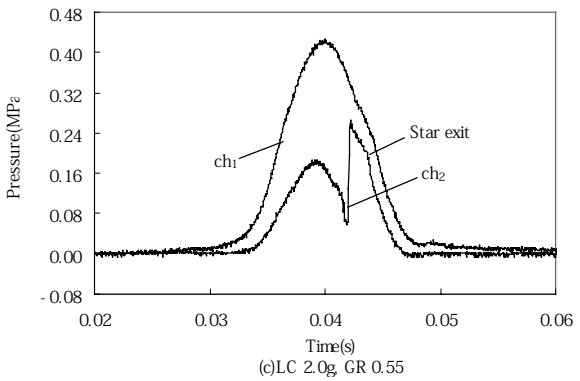

Fig. 3 *(a-c). Pressure profiles at the bottom and middle of the mortar*

The start time of the sharp pressure decrease at the middle transducer in this case was earlier than that at the bottom one. This indicates that the propagation of pressure was delayed more at the bottom than in the middle.

Figure 3(c) shows an experimental result with same LC (2.0 g) and larger GR (0.55) than Figure 3(b). The pressure differences at the bottom and middle transducers increased after the star passed the middle transducer compared to Figure 3(b). This may be attributable to the combustion gas passeing through the larger gap between the mortar wall and the star than the cases in Figures 3(a) and (b).

Reproducibility of the pressure profiles

It is important to know the effect of the mass of the lifting charge, the gap ratio between the mortar wall and the star, etc. on the muzzle velocity of the star. However, it is necessary to know the reproducibility of the data observed under the same condition, in order to understand the relationships correctly.

The following were selected as parameters describing characteristics of the pressure profile: The maximum pressure (P_{1max}), the muzzle pressure (P_{1muz}), the time to maximum pressure (t_{1max}), and the time to muzzle (t_{1muz})by the bottom transducer.

The statistical values of the parameters are listed in Table 1. Here, SD and RSD are standard deviation and relative standard deviation (SD/mean).

Table 1. *Statistical values of P_{1max},P_{1muz},t_{1max} and t_{1muz}.*

GR	*n*	Parameter	Mean	SD	RSD
0.28	6	P_{1max}	533 kPa	68.8 kPa	0.13
		P_{1muz}	521 kPa	67.5 kPa	0.13
		t_{1max}	11.6 ms	1.21 ms	0.10
		t_{1muz}	12.3 ms	1.06 ms	0.09
0.55	5	P_{1max}	295 kPa	79.7 kPa	0.27
		P_{1muz}	212 kPa	38.6 kPa	0.18
		t_{1max}	14.8 ms	2.97 ms	0.20
		t_{1muz}	18.1 ms	2.54 ms	0.14
0.71	5	P_{1max}	253 kPa	65.6 kPa	0.26
		P_{1muz}	102 kPa	74.2 kPa	0.72
		t_{1max}	14.5 ms	3.12 ms	0.21
		t_{1muz}	22.3 ms	4.80 ms	0.21

The scatter of the maximum pressure is larger than that of the time to maximum pressure. The maximum pressure and the time to maximum pressure both decrease with decreasing gap ratio.

Effect of gap ratio

The ratio of the escaped gas from the gap to total combustion gas increases with increasing gap

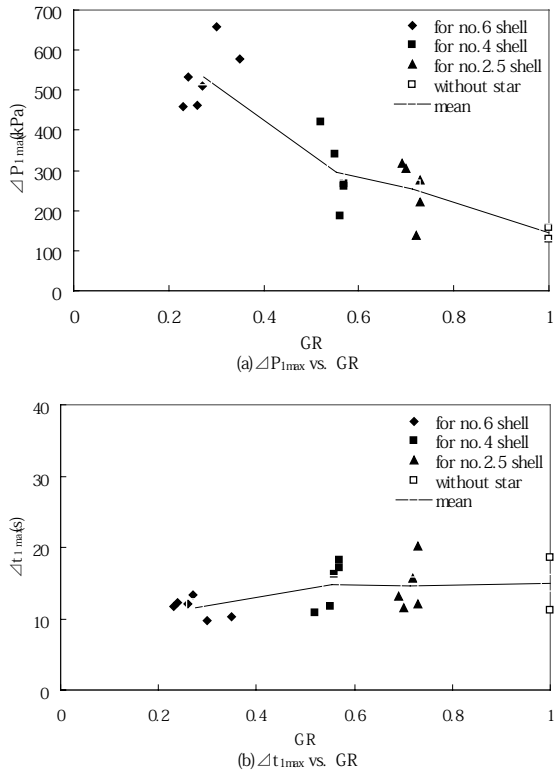

Figure 4(a)–(b). *Plots of P_{1max} and t_{1max} vs. GR.*

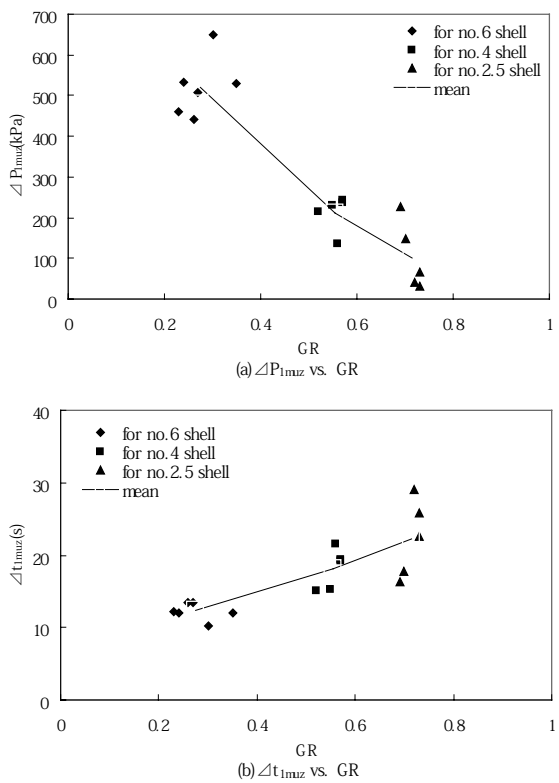

Figure 5(a)–(b). *Plot of P_{1muz} and t_{1muz} vs. GR.*

ratio. Figure 4 shows the plot of P_{1max} and t_{1max} against gap ratio.

The maximum pressure increased with a decrease in the gap ratio. This trend is more noticeable fora smaller gap ratio. The mean values of the time to maximum pressure were similar for GR of 0.55 and 0.71. However, they decreased considerably when the GR was 0.28.

Figure 5 shows a plot of P_{1muz} and t_{1muz} against GR. P_{1muz} decreased monotonously with increasing GR in contrast to the case of P_{1max}. t_{1muz} increased monotonously with increasing GR.

The following changes were observed in the pressure profiles at the bottom transducer of the mortar with 20 mm inner diameter and 361 mm depth using 2.0 g lifting charge, when the gap ratio was changed from 0.28 to 0.71. The star left the muzzle just after the time to maximum pressure when GR was 0.28. On the other hand, in the case of GR = 0.55 the star stayed longer in the mortar after the maximum pressure was attained. When GR was 0.71, the time during which the star stayed in the mortar became longer after the maximum pressure attained.

The following were also observed in the pressure profiles recorded by the middle transducer with the change in GR: no pressure increase was observed before the star passed the transducer when the lifting charge mass and GR were 1.0 g and 0.28, respectively. A pressure increase was observed before the star passed the transducer when the lifting charge and GR were 2.0 g and 0.28, respectively, but the increase was small. With 2.0 g lifting charge and 0.55 GR, the pressure increase before the star passed the transducer was more remarkable and with 0.71 GR much more remarkable.

The pressure increase before the star passed the middle transducer may be attributable to the combustion gas escaping through the gap between the mortar wall and the star. This may be supported by the pressure profiles recorded in the firing experiment using the same mortar without a star (Figure 8).

Effect of the mass of lifting charge

Experiments with different masses of lifting charge were carried out. Though there is some scattering

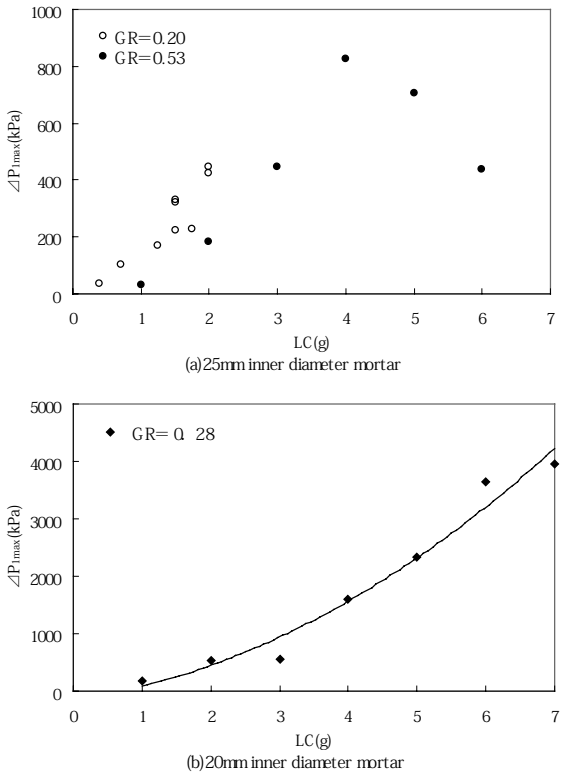

Figure 6. *Plot of P_{1max} vs. LC for (a) 25 mm mortars and (b) 20 mm mortars.*

of the experimental data, the maximum pressure increased with increasing lifting charge. Figure 6 shows the plot of $P_{1\max}$ against the mass of the lifting charge, using the mortars of 20 mm and 25 mm inner diameters.

$P_{1\max}$ increased with increasing mass of lifting charge with one exception. At the moment the reason for the exception is not clear.

Pressure profiles for the real pressures acting on a star using four transducers

It was found that, when the gap ratio became larger, the difference between the bottom and middle pressures became larger. Therefore, we carried out an experiment using a mortar equipped with four pressure transducers. The mortar was a steel tube of 20 mm inner diameter and 361 mm depth. The pressure transducers are situated at 11 mm, 131 mm, 251 mm and 346 mm from the bottom of the mortar (Figure 1). Examples of the recorded pressure profiles are shown in Figure 7.

The pressure profiles of ch1, ch2, ch3 and ch4 were different from each other when GR and LC were 0.71 and 2.0 g, respectively. Here, P_1, P_2, P_3 and P_4 are pressures recorded by ch1, ch2, ch3 and ch4 pressure transducers, respectively.

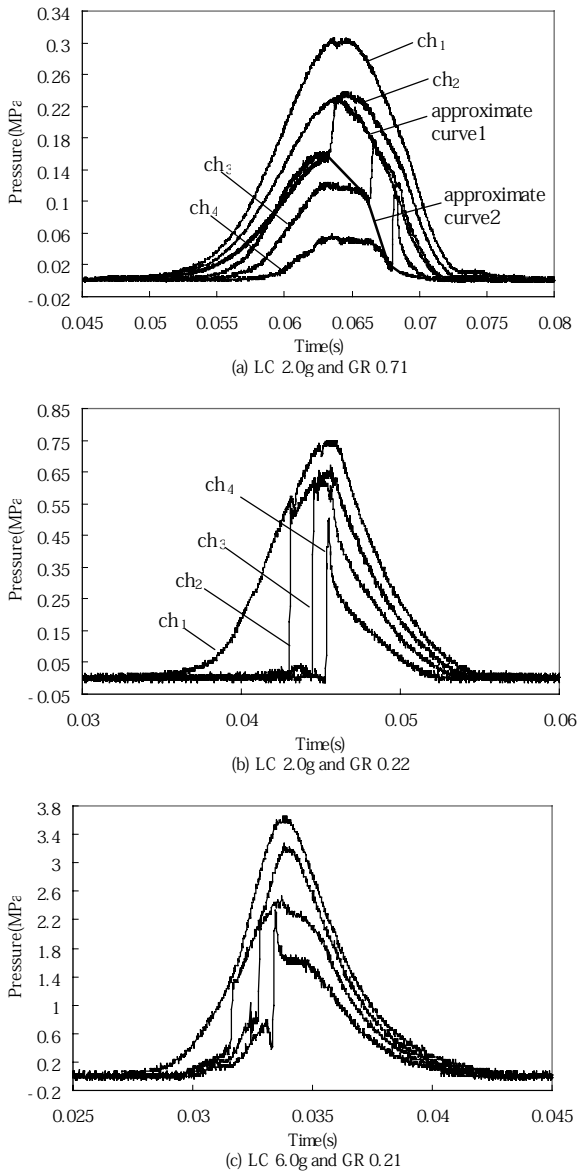

Figure 7. *Examples of the pressure profiles observed by four pressure transducers.*

These profiles may be explained as follows: the pressure P_1 recorded by ch1 reaches a maximum pressure $P_{1\max}$ after $t_{1\max}$ and the muzzle pressure P_{1muz} after t_{1muz}. P_2 recorded by ch2 reaches $P_{2\max}$ after $t_{2\max}$, then P_2 jumps to higher pressure and then reaches P_{2muz} after t_{2muz}. This pressure profile is different from that of ch1. The pressure measured at ch1 is always behind the star, but initially the pressure at ch2 is in front of the star and later behind the star.

These results indicate that the profile of P_1 is not

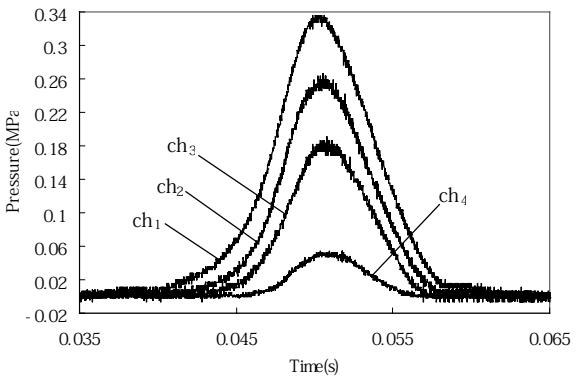

Figure 8. *Pressure profiles of four channels in the mortar on firing with no star.*

necessarily the true pressure profile acting on the rear surface of the star. If the time when the star passes ch2 is t_{ch2}, the real pressure acting on the rear surface of the star is not P_1 but P_2 at t_{ch2}.

Similarly, the real pressure acting on the rear surface of the star is neither P_1 nor P_2 but P_3 at t_{ch3}. The situation is same in ch4. Therefore, the real pressure profile acting on the rear surface of the star is a curve combining P_1, P_2, P_3 and P_4 at t = 0, t_2, t_3 and t_4, respectively. The pressure increases recorded at ch2, ch3 and ch4 before the star passes the respective channel are caused by the pressure in front of the star due to the combustion gas of the lifting charge escaping through the gap between the mortar wall and the star. The pressures decrease in the order: $P_1 > P_2 > P_3 > P_4$. The real pressure acting on the front surface of the star is the pressure at the time just before the sharp increase of pressure in each channel. Therefore, the real pressure profile for the front surface of the star is a curve joining these points. The real driving force is the difference between the above two acting pressures.

The pressure transducer of ch4 is situated near the muzzle of the mortar. The star leaves the muzzle just after it passes the transducer. The onset times of the sharp pressure decrease, t_{muz} , decrease in the order: $t_{1muz} > t_{2muz} > t_{3muz} > t_{4muz}$. The real time when the star passes the muzzle is not t_{1muz}, t_{2muz} or t_{3muz}, but near t_{4muz}.

Effect of the gap ratio GR

In the pressure profiles with GR 0.22–0.27 and LC 2.0 g (Figure 7(b)), the pressure differences of ch1, ch2, ch3 and ch4 are small before the star reaches the respective transducer, compared to the case of GR 0.71 and LC 2.0 g. Furthemore there is nearly no pressure increase in front of the star. This is due to little gas escaping owing to the small gap between the mortar wall and the star. On the other hand, the times of the sharp pressure increases of ch2, ch3 and ch4 decreased when GR was decreased from 0.71 to 0.22–0.27. This may be due to the higher rear gas pressure and higher velocity of the star because of the smaller gap between the mortar wall and the star for lower GR.

We carried out a firing experiment without a star using the mortar with four pressure measuring channels, GR 1.0 and LC 2.0 g. The pressure profiles (Figure 8) look like those of the case where GR = 0.71 and LC = 2.0 g with a star (Figure 7(a)).

Effect of lifting charge mass LC

The pressure profiles (Figure 7(c)) with GR 0.21–0.30 and LC 6.0 g are more different from those (Figure 7(b)) with GR 0.22 and LC 2.0 g, regarding the pressures of all the channels. On the other hand, the times to the sharp pressure increase were shorter than in the case of Figure 7(b). One of the characteristics of the experiment with GR 0.21–0.30 and LC 6.0 g is that the pressure in the mortar remained after the star left the muzzle. This can be seen from the pressure profile of ch4. The pressure of ch4 increases sharply when the star passes near the muzzle. In the experiment with LC 2.0 g, the pressure of ch4 decreased sharply and monotonously. But, in the experiment with LC 6.0 g, the pressure of ch4 decreased initially, but fairly high pressure remained thereafter. This may be due to the continuation of the combustion of lifting charge after the star left the muzzle.

Reproducibility of experiment

Table 2 lists the time to maximum pressure of ch1 t_{1max}, the maximum pressure P_{1max} and their relative standard deviations in the four channel experiments with stars.

In firing stars, the scatter of the times to maximum pressure increased with increasing gap ratio. Regarding the scatter of the maximum pressures, no effect of the gap ratio was observed with LC 2.0 g. With LC 6.0 g, the scatter of both t_{max} and. P_{max} were small.

Table 2. *Time to maximum pressure t_{1max}, maximum pressure P_{1max} and relative standard deviations RSD of the ch1 in star firing*

GR	0.69–0.72	0.22–0.27	0.21–0.30
LC	2.0 g	2.0 g	6.0 g
t_{1max}	12.7 ms	9.32 ms	4.34 ms
RSD	0.28	0.02	0.07
P_{1max}	253 Pa	619 Pa	3704 Pa
RSD	0.30	0.29	0.05

Table 3 shows t_{max}, P_{max} and the relative standard deviations recorded by the four pressure transducers in firing with no stars.

Table 3. *Time to maximum pressure t_{max}, maximum pressure P_{max} and relative standard deviations RSD of the data from all four channels in firing with no star (GR 1.00 and LC 2.0 g)*

ch1	t_{1max}	11.1 ms
	RSD	0.28
	P_{1max}	239 Pa
	RSD	0.43
ch2	t_{2max}	11.38 ms
	RSD	0.28
	P_{2max}	174 Pa
	RSD	0.53
ch3	t_{3max}	11.57 ms
	RSD	0.28
	P_{3max}	119 Pa
	RSD	0.61
ch4	t_{4max}	11.74 ms
	RSD	0.28
	P_{4max}	49 Pa
	RSD	0.83

In the case of firing with no star, the maximum pressures decreased from 239 kPa (ch1) to 49 kPa (ch4), and the relative standard deviation increased from 0.43 (ch1) to 0.83 (ch4). The time to maximum pressure increased slightly from 11.10 ms (ch1) to 11.74 ms (ch4) and the relative standard deviations were 0.28 without change.

Motion of a star in the mortar[3]

The equations of a star in the mortar are expressed as follows:

$$M\frac{\mathrm{d}u}{\mathrm{d}t} = p(t)\times A - Mg \qquad (1)$$

$$\frac{\mathrm{d}Z}{\mathrm{d}t} = u \qquad (2)$$

Here, M, u, A, and Z are mass, motion velocity, maximum cross sectional area, and traveling distance of the star, respectively.

$$A = \frac{\pi D^2}{4} \qquad (3)$$

Here, D is the diameter of the star, and equation (1) can be rewritten as follows:

$$\frac{\mathrm{d}u}{\mathrm{d}t} = \frac{\pi D^2}{4M}\cdot p(t) - g \qquad (4)$$

Here, $p(t)$ is the observed value and substituted into Equation (4).

Equations (3) and (4) are simultaneously solved by numerical calculation, and acceleration du/dt, velocity u and traveling distance Z are obtained.

Observed initial velocity of the star in the air and calculated muzzle velocity

When a star is fired, smoke and flame appear from the muzzle and then the star appears above the smoke. We can only determine initial velocity after the star appears from the smoke. In the same experiment with the pressure measurement, observed initial velocities were compared with calculated muzzle velocities from the pressure profiles in the mortar.

Table 4 and Table 5 list observed initial and calculated muzzle velocities of stars using 25 mm ø and 20 mm ø mortars, respectively.

Figure 9 and 10 show plots of calculated muzzle velocity *vs*. observed initial velocity of stars with 25 mm ø and 20 mm ø mortars, respectively.

In Figure 9 the calculated muzzle velocity agreed fairly well with the observed initial velocity of the star. On the other hand, in Figure 10 it can be

Table 4. *Observed initial and calculated muzzle velocities of stars using 25 mm ø mortar.*

Run no.	Star	Mass/g	Diameter/mm	Lifting charge/g	Gap ratio	Initial velocity/m s^{-1} obs.	cal.
1	no. 10 shell	9.517	22.701	0.40	0.18	27	26
2	no. 10 shell	9.065	22.318	0.70	0.20	57	56
3	no. 10 shell	8.308	22.353	1.25	0.20	77	80
4	no. 10 shell	8.846	22.626	1.50	0.18	86	92
5	no. 10 shell	8.346	21.756	1.50	0.24	103	113
6	no. 10 shell	8.924	22.410	1.50	0.20	106	111
7	no. 10 shell	8.475	22.045	1.75	0.22	91	89
8	no. 10 shell	9.244	22.166	2.00	0.21	117	121
9	no. 10 shell	8.589	22.511	2.00	0.19	117	138

Table 5. *Observed initial and calculated muzzle velocities of stars using 20 mm ø mortar.*

Run no.	Star	Mass/g	Diameter/mm	Lifting charge/ g	Gap ratio	Initial velocity/m s^{-1} obs.	cal.
1	no. shell 6	3.770	16.686	1	0.30	80	86
2	no. shell 6	3.791	17.175	2	0.26	116	
3	no. shell 6	3.742	16.917	3	0.28	131	148
4	no. shell 6	4.084	17.441	4	0.24	167	264
5	no. shell 6	3.310	16.561	5	0.31	145	423
6	no. shell 6	3.847	16.666	6	0.31	190	443
7	no. shell 6	3.705	17.112	7	0.27	195	890
8	no. shell 6	3.908	17.126	2	0.27	119	141
9	no. shell 6	4.002	17.535	2	0.23	138	131
10	no. shell 6	3.520	16.179	2	0.35	134	167
11	no. shell 6	4.070	17.482	2	0.24	121	129
12	no. shell 6	3.751	16.706	2	0.30	126	155
13	no. shell 4	1.868	13.373	2	0.55	93	192
14	no. shell 4	1.838	13.299	2	0.56	83	149
15	no. shell 4	1.836	13.160	2	0.57	104	142
16	no. shell 4	1.984	13.813	2	0.52	104	236
17	no. shell 4	1.813	13.161	2	0.57	90	149
18	no. shell 2.5	0.893	10.342	2	0.73	65	215
19	no. shell 2.5	0.847	10.508	2	0.72	40	187
20	no. shell 2.5	0.898	10.418	2	0.73	39	249
21	no. shell 2.5	1.070	11.088	2	0.69	90	206
22	no. shell 2.5	1.026	10.966	2	0.70	79	251

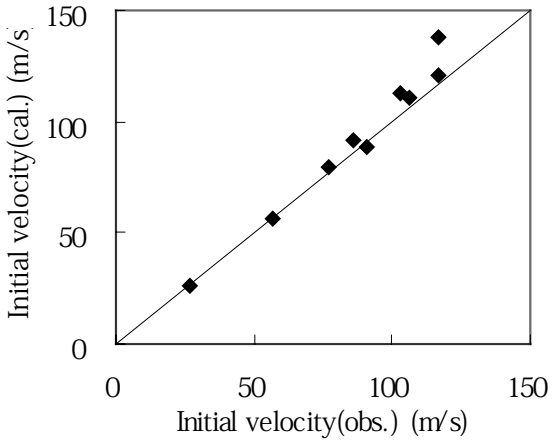

Figure 9. *Plot of calculated muzzle velocity vs. observed initial velocity of star with 25 mm ø mortar.*

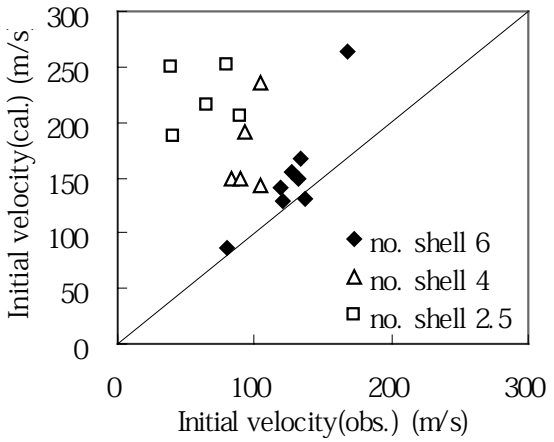

Figure 10. *Plot of calculated muzzle velocity vs. observed initial velocity of star with 20 mm ø mortar.*

seen that the calculated values deviate more from the observed one with the smaller star and more lifting charge.

Correlation of the muzzle velocity of star with the mass of lifting charge

The relationships between the initial velocity of stars and the mass of lifting charges are shown in Figure 11 and Figure 12. Generally, the initial velocity of star increases with the increasing mass of lifting charge, but the increase in the initial velocity weakened when the mass of lifting charge exceeded 2 g.

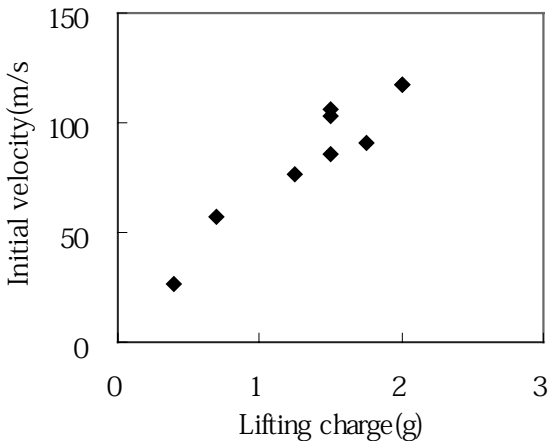

Figure 11. *Plot of the initial velocity vs. the mass of lifting charge with the 25 mm ø mortar and the stars for no.10 shell.*

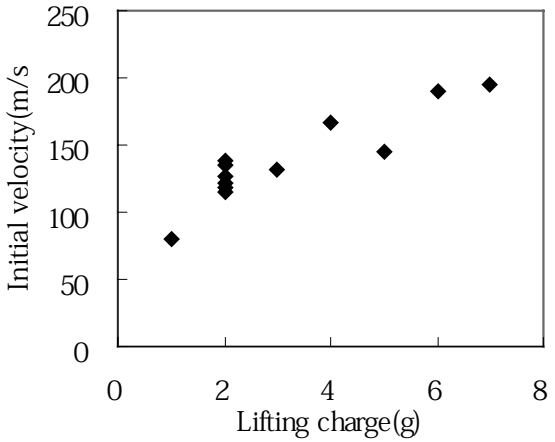

Figure 12. *Plot of initial velocity vs. the mass of lifting charge with the 20 mm ø mortar and the stars for no.6 shell.*

Effect of the gap ratio on the initial velocity of star

Figure 13 shows the plot of the initial velocity of a star against the gap ratio. It was found that the observed initial velocity decreased and the scatter of the initial velocity increased with increasing gap ratio.

Estimation of the muzzle velocity of star considering the pressure distribution in the mortar

The calculated muzzle velocities of the stars with and without correction for the pressure distribution in the mortar are listed in Table 6. The corrected

Table 6. *Observed initial and calculated muzzle velocities of stars using the 20mmφ mortar with 4 pressure transducers*

Stars				Calculated muzzle velocity/ m s^{-1}		
Mass/g	Diameter/mm	Lifting charge/g	Gap ratio	Without correction	With correction	Measured muzzle velocity/m s^{-1}
0.986	10.682	2.0	0.71	254	66	78
4.780	17.696	2.0	0.22	146	136	129
4.757	17.696	2.0	0.22	169	154	135
4.199	17.067	2.0	0.27	145	115	114
4.699	17.553	2.0	0.23	155	134	135
4.155	17.737	6.0	0.21	414	255	233
3.916	17.420	6.0	0.24	361	227	209
3.607	17.041	6.0	0.27	422	249	213
3.644	16.737	6.0	0.30	394	219	209
3.632	16.795	6.0	0.29	388	221	200

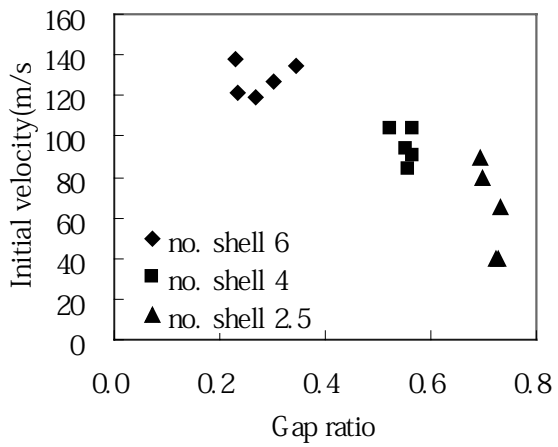

Figure 13. *Plot of initial velocity vs. GR.*

calculated values are in better agreement with the observed initial velocities than the values without correction when the gap ratio was large. In the case of small gap ratio and small mass of lifting charge, the difference between the calculated muzzle and observed initial velocities is small and the effect of the pressure distribution is also small. Therefore, the muzzle velocity of the star is estimated most accurately from the pressure profile at the bottom of the mortar when the gap ratio and the mass of lifting charge are small.

Acknowledgment

The authors wish to gratefully acknowledge the experimental assistance of Sunagaga Fireworks Company, Showarika Company, and the undergraduate students of Higaki Laboratory: Arima, Ariga, Kashiwa and Hukazawa.

References

1 D. Ding, M. Higaki and T. Yoshida, "Burning and Air Resistance of Fireworks Stars", *Science and Technology of Energetic Materials*, in press.

2 K. L. Kosanke and B. J. Kosanke, "Peak In-Mortar Aerial Shell Accelerations", *Journal of Pyrotechnics*, Issue 10, 1999, p. 56.

3 Y. Ooki, D. Ding, M. Higaki, and T. Yoshida, "Interior Pressure in the Mortar and Motion of a No. 3 Shell in a Fireworks Shot", *Journal of Pyrotechnics*, Issue 22, 2005, pp. 3–8.